DELIVERABLE REPORT

Project acronym: INPUT
Project number: 687795

D5.3, Factors of influence on EMG features for myocontrol

Dissemination type:	R
Dissemination level:	PP
Planned delivery date:	2018-01-31
Actual delivery date:	2018-02-06
Reporting Period:	1

WP5, Task 5.2, Modelling factors of influence on the surface EMG

Lead: UMG-ICL

1 DESCRIPTION OF THE TASK

The following description is taken from Annex I:
ALTHOUGH IT IS WELL KNOWN THAT EMG IS SENSITIVE TO MANY FACTORS OF INFLUENCE, THE WAY IN WHICH THE CHARACTERISTICS OF THE EMG CHANGE WITH THESE FACTORS HAS STILL TO BE CLARIFIED. IN THIS WORK-PACKAGE, A LARGE SET OF SIMULATIONS WILL BE USED TO DESCRIBE IN DETAIL THE CHANGES IN EMG FEATURES WITH CHANGES IN ELECTRODE LOCATION, MUSCLE FATIGUE, ETC. THE MODELLING WORK WILL BE COMPLEMENTED BY EXPERIMENTS THAT WILL COVER SOME OF THE VALIDATION ASPECTS. FINALLY, EACH FACTOR OF INFLUENCE WILL BE INVESTIGATED WITH VARIOUS ELECTRODE CONFIGURATIONS, LINKING THIS SUBTASK TO THE TASK 5.1. THE MAIN FACTORS OF INFLUENCE THAT WILL BE MODELED ARE ELECTRODE SHIFT, CHANGE IN THE SPATIAL DISTRIBUTION OF MUSCLE ACTIVITY, CHANGES IN ELECTRODE IMPEDANCE, AND MUSCLE FATIGUE. AMONG THESE, EXPERIMENTAL VALIDATION WILL FOCUS ONLY ON THE CHANGE IN THE SPATIAL DISTRIBUTION OF MUSCLE ACTIVITY AND FATIGUE, WHICH CAN BE RE-CREATED IN THE LAB.

DESCRIPTION OF DELIVERABLE

The deliverable includes comprehensive description of the effect of muscle fatigue on the control signals used for regression-based myoelectric control obtained by means of simulations. The deliverable also experimentally investigates the influence of donning and doffing, which includes changes in electrode skin-contact. Changes in the EMG signals due to electrode shift have been intensively investigated in Deliverable 5.1 and therefore will not be investigated here.

2 IMPLEMENTATION OF WORK

The work was divided into two parts devoted to investigate the effect of muscle fatigue and the influence of donning and doffing in a myoelectric control task based on regression. The

choice of the control algorithm stems from the recommendation reported in Deliverable 5.1 that systems based on regression of EMG features have to be preferred over classification in the development of the INPUT myocontrol system. The regression system was based on non-negative matrix factorization (NNMF). NNMF has been used in several studies on regression based myoelectric control (Jiang et al., 2009; Muceli et al., 2014). NNMF allows extracting control signals in an unsupervised manner from EMG signals. Therefore, this method was employed rather than alternative methods such as neural networks that require labeling data, such as kinematics. Also, NNMF allows the extraction of weights that may be linked to specific muscle/electrode positions and thus easily interpreted compared to the weights used in other methods, such as linear regression or neural networks. In any case, the obtained results can be considered generally for regression methods (Hahne et al., 2014). The experimental study relies on able-bodied subjects (this work was conducted before the review meeting when it was decided to focus the experiments on amputees). For this basic research question the particular user group was not as relevant as in applied ADL tests, for example.

3 SIMULATION STUDY ON MUSCLE FATIGUE

Model of muscle fatigue

To investigate the effects of muscle fatigue on a regression-based myoelectric control system, we considerably extended the model presented in Deliverable 5.1. With respect to that model that considered only one active muscle, in the model presented in this deliverable we simulated 7 active muscles which corresponds to the superficial layer of the forearm (flexor carpi radialis, flexor carpi ulnaris, pronator teres, extensor carpi radialis longus, extensor carpi radialis brevis, extensor carpi ulnaris).

The model describes the volume conductor as a multilayered cylinder. It was assumed that the forearm had a circumference of 24 cm and thus a radius of 3.82 cm. Four layers were simulated to describe the bone, muscle tissue, fat and skin. Skin and fat thickness were set to 1 and 2 mm, respectively. The presence of the radius and ulna bones was translated in simulations as a circular bone tissue of 7.5 mm in the central part of the cylinder. It was assumed that the forearm is about 27 cm long and that the fiber length corresponds to 20 cm along the forearm length. The muscle was more conductive in the longitudinal than in the transversal fiber direction (conductivity ratio 5). The conductivity ratios skin/fat layers and fat/muscles were 20 and 0.5, respectively (Keenan et al., 2006).

It was assumed that 2800 motor units are scattered in random positions within the annulus representing the muscle. Each motor unit had a number of fibers in the range 5-70 (exponential distribution). The number of motor units per muscle was in the range 80-200. The radius of each muscle was determined from the root square of the number of motor units constituting the muscle. Figure 1 shows the simulated motor unit population and an example of the 7 muscles located within the forearm.

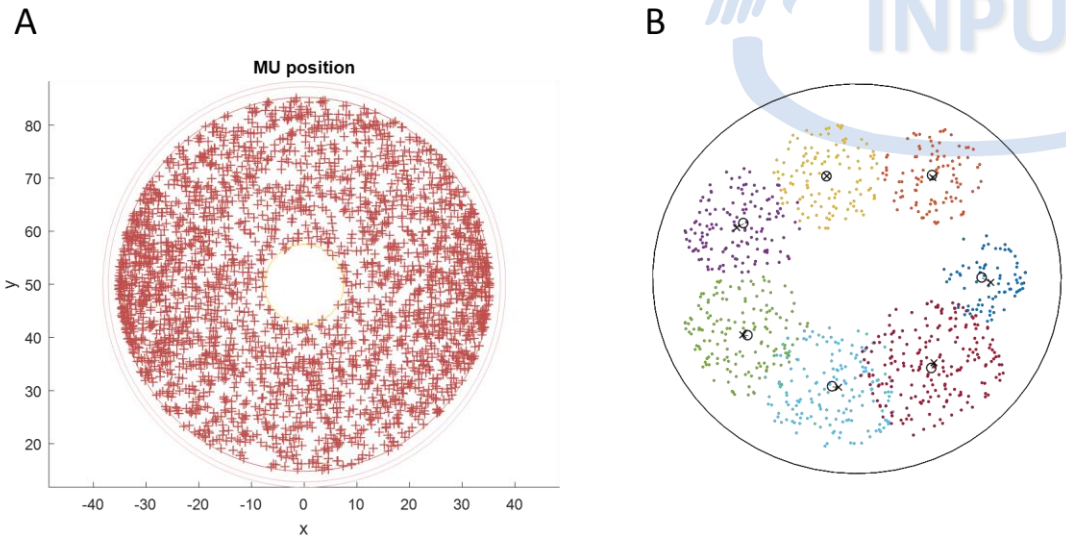

Figure 1 Simulated motor unit population. A) Four layer model, the inner layer represent the bone, the outer layers the skin and the adipose tissue. Between the inner and outer layer is the muscle tissue with the muscle fibers randomly scattered. B) Example of the subdivision of the motor unit population in 7 superficial muscles. Each dot represents the center of a motor unit territory.

The detection system was a 24x8 grid of circular electrodes with 3 mm diameter. Monopolar recordings were obtained from the simulations and combined according to the spatial filters used with the experimental data. The sampling frequency was set to 4096 Hz.

The simulation parameters are summarized in the following Table.

Model parameters	Values
Muscle tissue properties	
Muscle cross section (radius)	38.2 mm
Number of motor units	2800
Number of fibers in a motor unit (range)	5–70
Skin thickness	1 mm
Subcutaneous tissue thickness	2 mm
Average fiber length	200 mm
Innervation zone (location along fiber from proximal to distal attachment)	50%
Innervation zone and tendon spread	5 mm
Conductivity ratios	
Skin and subcutaneous tissue	20
Subcutaneous tissue and muscle	0.5
Muscle—longitudinal and transversal to fiber direction	5
Number of motor units per muscle	
Detection system	Monopolar
Electrode shape and diameter	Circular, 3 mm
Interelectrode distance	10 mm
Center of detection system (location along fiber from innervation zone to distal attachment)	60%

An integrate-and-fire model was adopted to calculate the motor unit output in response to input. The motor unit firing thresholds were drawn from an exponential distribution (Fuglevand et al., 1993). The range of recruitment thresholds was set to be 8-fold.

The input to each muscle comprised three components: common (to the whole motoneuron pool) input and common noise, and independent noise (Negro and Farina, 2011). The noise was simulated as white Gaussian noise in the bandwidth 100-120 Hz.

The simulations included 10 datasets that differed for the position of the muscles in the forearm circumference and the synergy matrix, to take into account for randomly assigned parameters. Each dataset included a baseline condition and a fatigue condition. Fatigue is known to cause changes both at the peripheral and central level and in the current model was simulated varying two parameters: the motor unit conduction velocity and their recruitment threshold.

Conduction velocity of the muscle fiber action potentials is known to decrease with fatigue (Gazzoni et al., 2005). The conduction velocity of muscle fiber action potentials belonging to a motor unit were related to motor unit size. In the baseline condition the conduction velocity distribution was Gaussian with mean (SD) 4 (0.5) m/s (Keenan et al., 2005). In the fatiguing condition, the conduction velocity was scaled toward lower values (Figure 2).

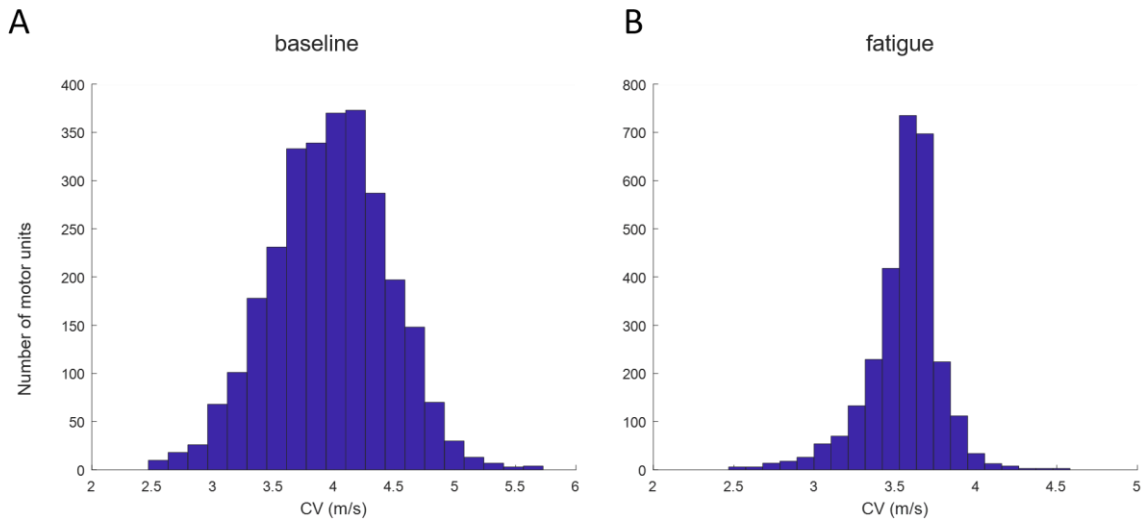

Figure 2 Conduction velocity distribution in the baseline (A) and fatigue (B) conditions. Conduction velocity was Gaussian with mean 4m/s (A) and scaled to the lower range to simulate fatigue (B).

Fatigue also causes the progressive recruitment of additional motor units (Bigland-Ritchie et al., 1983) to maintain force. This phenomenon was simulated by means of a decrease in the recruitment threshold (Figure 3).

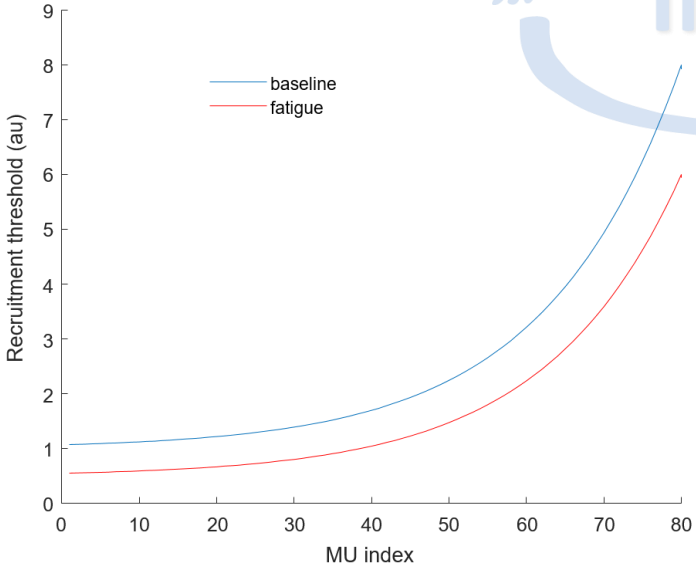

Figure 3 Representative example of the decrease of the recruitment threshold for one of the 7 muscles that was imposed to simulate the increase in motor unit recruitment observed in fatiguing contractions.

It was assumed that forearm muscles act in a synergistic fashion (Jiang et al., 2009), i.e. that the central nervous system controls multiple muscles in functional groups (synergies) rather than individually. According to this model, the activation of M muscles CI(t) (the common input according to the above notation) results from an instantaneous mixing between N (<M) activation signals (commands) F(t) and the gains S (M×N) by which the activation signals are transferred to the muscles (CI(t)=S·F(t)). In the simulations, N was set to 4, according to (Muceli et al., 2014). This corresponds to the activation of two degrees of freedom of the hand/wrist (e.g., flexion/extension and radial/ulnar deviation). M was set to 7, as the number of muscles. It was assumed that each movement was performed three times. Each burst of activity was simulated in the activation signals as a Gaussian with standard deviation in the range 0.1-0.2 of the sampling frequency. Figure 4 shows a representative example of the muscle synergy framework.

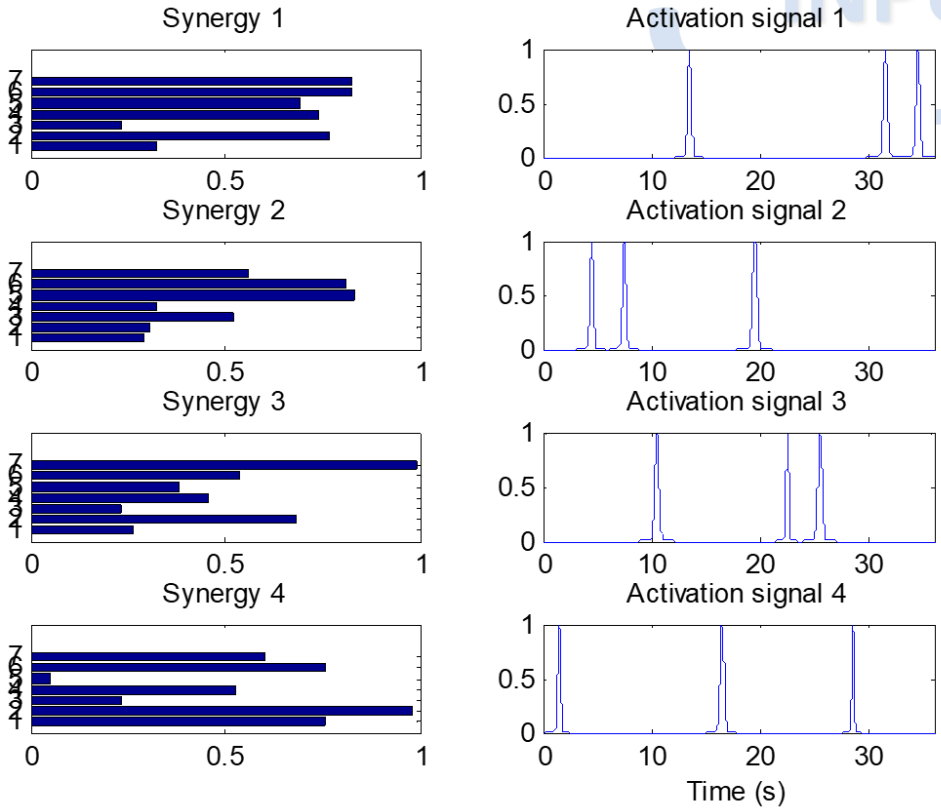

Figure 4 Representative example of muscle synergies and activation signals imposed during a simulation. Four synergies were considered for two degrees of freedom. Each synergy represents the relative activation of 7 muscles. Each movement was repeated 3 times, corresponding to the three bursts in the activation signals.

Twenty-four bipolar channels around the forearm were selected for the analysis. Envelopes were extracted from the simulated EMG signals via low-pass filter with cut-off frequency at 5 Hz. EMG amplitude is known to increase with fatigue (Enoka et al., 2011) due to the recruitment of additional units. EMG envelopes obtained from the baseline and fatigue contractions were compared by means of the correlation coefficient and the area under the envelopes. Data are reported as mean and standard deviation across the 10 datasets.

EMG envelopes corresponding to the baseline condition were decomposed into synergies and activation signals using NNMF (Lee and Seung, 2006). The synergy matrix was determined with the DOF-wise approach proposed in (Jiang et al., 2009) that finds S as the concatenation of one matrix for each of the two degrees of freedom considered, obtained from the activation of one degree of freedom at a time. For each of the 10 datasets, the same (random) synergy matrix was imposed to both the baseline and fatigue condition. The synergy extracted from the baseline data was therefore used to analyze the data from to the fatigue condition. The synergy matrix was (pseudo)inverted and multiplied by the envelopes corresponding to the fatigue condition to obtain the corresponding activation signals. Activation signals obtained from the baseline and fatigue contractions were compared by means of the correlation coefficient and the area under the envelopes.

The analysis showed that fatigue resulted in an increase of the amplitude of the EMG signals that was reflected in an increase of the amplitude of the activation signals, as detailed in the following. Figure 5 shows a representative example of the myoelectric manifestation of fatigue.

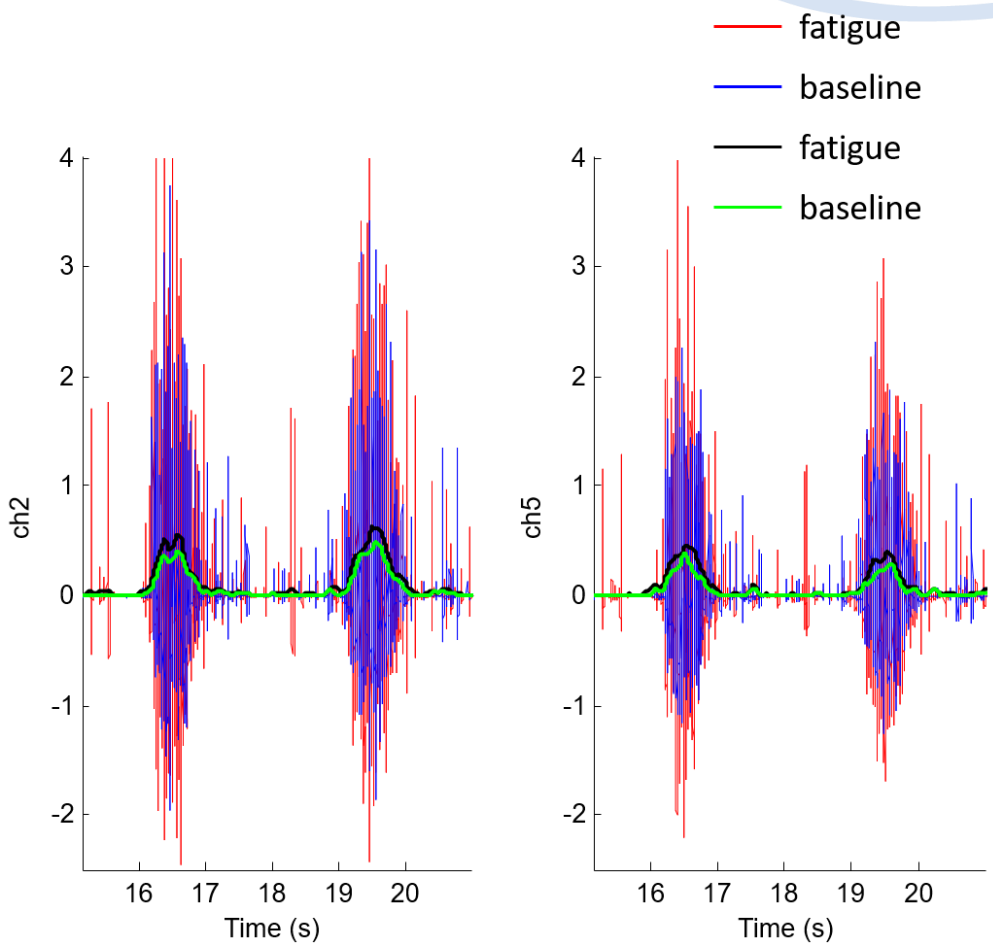

Figure 5 Change in EMG amplitude due to fatigue. Two representative channels are shown during the simulation of two movements. The EMG amplitude increased with fatigue as it can be observed both from raw EMG and the envelopes.

Envelopes corresponding to the fatigue condition had higher amplitude than the corresponding envelopes of the baseline condition in all 10 datasets (178.3±5.7%, according to the area).

Figure 6 shows an example of the activation signals imposed during simulations, and extracted from the baseline and fatigue conditions.

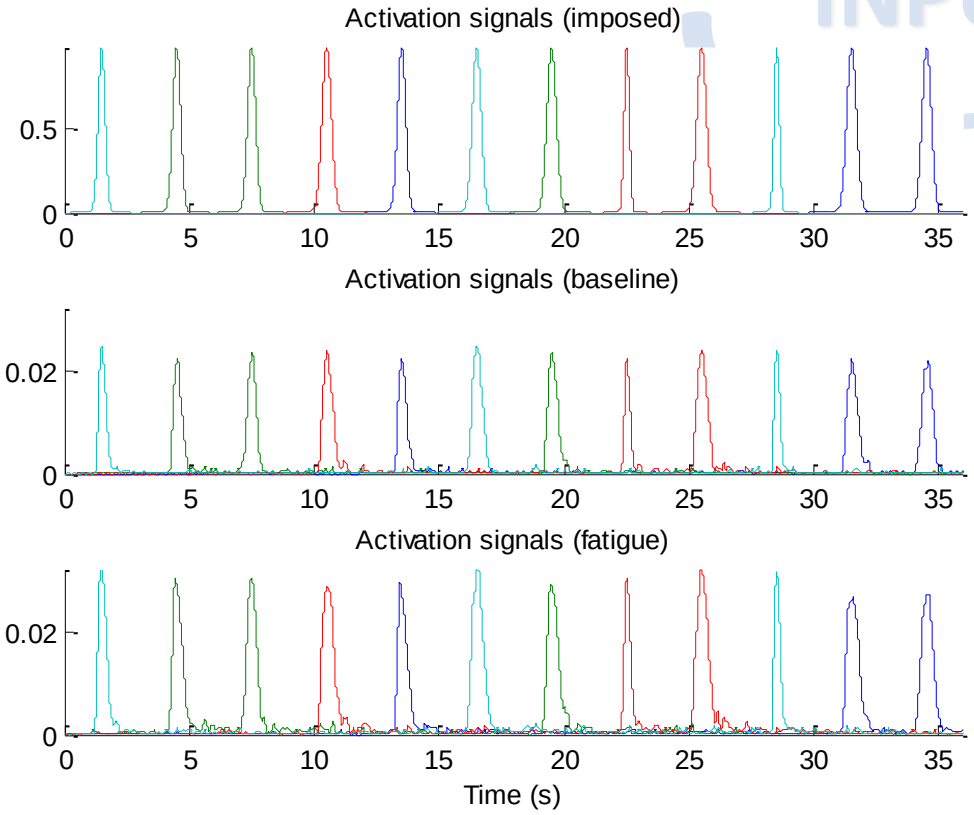

Figure 6 Top panel: activation signals imposed during the simulations, different colours correspond to different movements (i.e., 4 different activation signals are represented in each panel). Each movement was repeated 3 times. Middle panel: activation signals extracted via DOF-wise non-negative matrix factorization from the EMG envelopes corresponding to the baseline condition. Bottom panel: activation signals extracted from the fatigue condition using the synergies extracted from the baseline condition.

First, it can be observed that the activation signals extracted via the DOF-wise NNMF (middle panel) were similar to those imposed during simulation (top panel). A comparison of the amplitude between these two cases is meaningless as the results of NNMF as other factorization algorithms present the ambiguity of scaling (the activation signals can be scaled of any value provided that the synergy matrix is scaled of the inverse value). Therefore, we compared only the shape of the activation signals in the two cases. Average correlation values across the 10 datasets were 0.98±0.01.

The activation signals were similar to those of the baseline but higher in amplitude (note that the scale is the same in the middle and bottom panels of Figure 6). It is worth noting that the comparison of amplitudes is meaningful in this case as the synergy matrix was fixed and was the same in both conditions. Across the 10 datasets, the corresponding average values of correlation and amplitude were 0.99±0.00 and 167.9±5.9%, for the correlation and area respectively. This means that the change in EMG due to fatigue implied an increase in the activation signals.

Since the activation signals extracted with the DOF-wise approach directly correspond to the control signals (i.e. the degree of activation for each movement), from a practical point of view, the amplitude increase of the activation signals means that if an amputee would try to achieve the same force level in

the presence of fatigue, the corresponding control signal will be amplified. Therefore, in theory he/she should be able to accomplish the same task exerting less force.

Experimental validation

We tested the effect of muscle fatigue experimentally in a myoelectric control task (two subjects). The subject sat in a chair in front of a computer screen. Surface EMG signals were recorded using eight bipolar stainless steel dry electrodes, which were equally distributed around the maximum diameter of the right forearm. The subject was asked to keep their right arm relaxed, extended in the sagittal plane at the side of the body, with the hand in a neutral position (fingers pointing down and thumb facing the front). Signals were sampled at 200 Hz (8-bit accuracy) and digitally filtered by a fifth order Butterworth high- pass (5 Hz cut off frequency) and a fifth order Butterworth low pass (90 Hz cut off frequency). Powerline interferences at 50 Hz were cancelled by a second order band stop Butterworth. Data was queued in a 4 s buffer after pre-processing, to extract the features and display the feedback (updated every 40 ms). The root mean square (RMS) of each EMG channel was computed from the data buffer in windows of 160 ms, complying with the acceptable controller delay for the average prosthetic user (Farrell and Weir, 2007). The windows had 120 ms overlap due to the update rate of the controller.

An onscreen cursor with pre-defined trajectories in a two-dimensional coordinate system was presented to the subjects to guide them during movement execution. The horizontal axis was mapped to flexion/extension, the vertical, to radial/ulnar deviation and the origin to rest. The cursor moved at a constant speed from the origin to the 80% of the virtual reality axis of the corresponding movement in 1.2 s, dwelled for 0.5 s and returned to rest in 1.2s, where it stopped for 2.5 s. Between repetitions, subjects were allowed to rest for at least 3 s to avoid fatigue. Each DOF was repeated 4 times.

NMF was used to decompose the active muscle synergies and to create the online control mappings. Mapping directly the control estimate into a cursor position would result in a relatively unsteady control caused by the stochastic nature of EMG. Thus, a simple moving average filter was applied to compensate this effect. Its length was adjusted for each run between 5-7 samples to provide a smooth control. In addition, each direction of the output estimate was multiplied by a scaling factor, which was finely tuned to ensure that subjects could reach the entire area of the target display. The generated mappings were used for the real-time control of an onscreen cursor in a two-dimensional coordinate system in a goal-oriented fashion.

During each testing phase, twenty circular targets of 8 device-independent pixels (dp) appeared on screen. The targets followed two elliptic trajectories (Figure 7) with major and minor axes corresponding to (100% of the virtual reality horizontal axis, 75% of the virtual reality vertical axis) and (60% of the virtual reality horizontal axis 45% of the virtual reality vertical axis), respectively. Targets in the outer ellipse were placed at angles of 7, 37 and 77 degrees; mapped to the other quadrants by adding 90, 180 and 270 degrees, respectively (see Figure 7). The inner ellipse targets were set at angles of 17 and 61 degrees, mapped to the remaining quadrants as mentioned before. The targets' order of appearance was randomized for each experiment.

In each trial two targets were shown: the current one in a thick solid line and the next target in a thin dotted line for preparation. To hit a target successfully, it had to be reached in less than 20 s and dwelled inside it for 300 ms. The subjects were asked to rest between targets, so the cursor was always at the origin at the beginning of the trials.

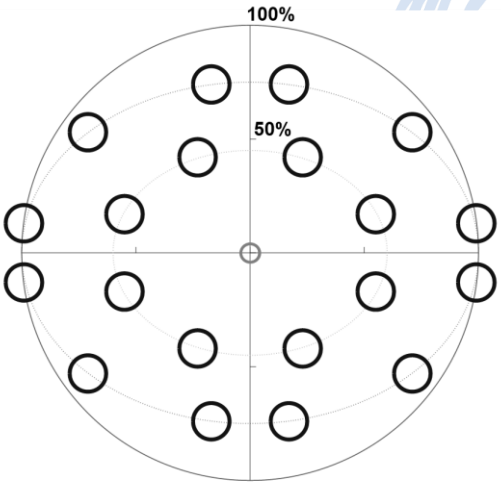

Figure 7 Target distribution in the subjects' feedback window. The solid line represents the circumference of MVC, and the dotted lines the target elliptical trajectories. Black circles correspond to the targets. The small grey in the origin is the cursor. The horizontal axis was mapped to Extension (positive direction) and Flexion (negative direction). Similarly, the vertical axis was mapped to Radial deviation (positive) and Ulnar deviation (negative).

The task of this experiment was the real-time myoelectric control of the onscreen cursor using different synergy mappings.

To quantify the performance of the real-time control system, six predefined metrics (defined in the Table below) were calculated (Kamavuako et al., 2014): completion rate, completion time, throughput, path efficiency, average speed and overshoot.

DEFINITIONS OF THE REAL-TIME PERFORMANCE METRICS

Metric	Definition
Completion Rate (CR)	Rate between the number of successfully reached and total targets
Completion Time (CT)	Average time needed to hit a target successfully
Index of Difficulty (ID)	$ID = \log_2(1 + \text{target distance}/\text{target width})$
Throughput (TP)	Mean of means of the ratio between the Index of Difficulty and the Completion Time
Path Efficiency (PE)	Ratio between the straight-line distance to the target and the distance of the path taken to hit it
Average Speed (AS)	Average non-zero speed of the cursor during the trial
Overshoot (OS)	Number of times the cursor entered the target and left before the 300 ms dwell time, normalized by the total number of targets

Once the subject completed the task, fatigue was induced via co-contraction of the forearm flexor and extensor muscles for 3 minutes. The subject repeated the same myocontrol task using the synergy matrix extracted during the baseline condition. After reaching each target, the subject co-contracted for 30 s to ensure that fatigue persisted for the entire duration of the hitting task. No EMG could be stored during the task due to real-time implementation constraints. However, the subjects were asked to perform a flexion/extension and a radial/ulnar deviation movement at the end of the fatigue task and the corresponding EMG had higher amplitude than that recorded during the algorithm training confirming that fatigue was actually present.

The myocontrol task was repeated again 20 minutes after in the absence of fatigue to rule out the effect of learning in the performance. Figure 8 shows that performance was unchanged by the fatigue condition. Thus, the subject was able to adapt to the change in condition during the real-time task.

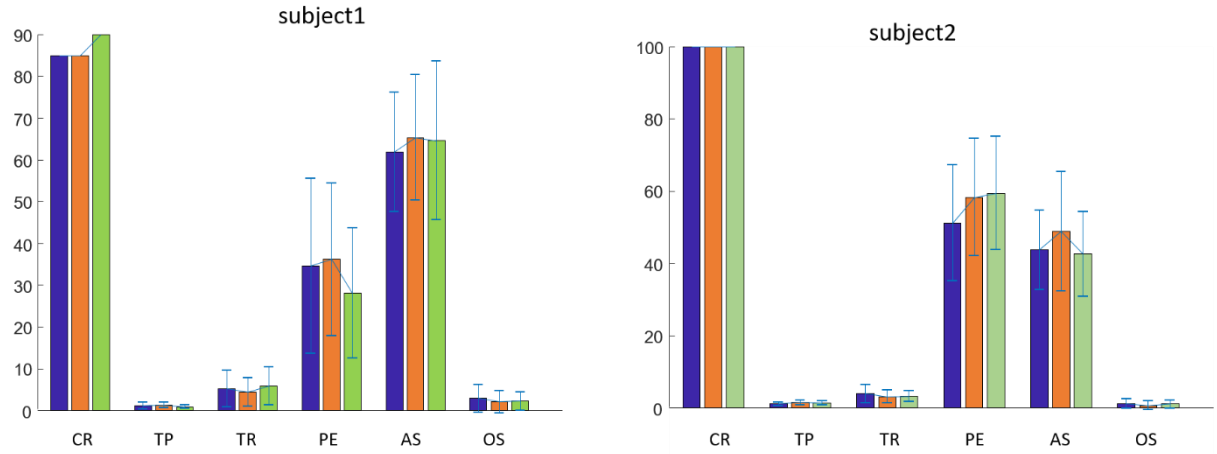

Figure 8 Average performance across targets in the baseline (blue), fatigue (orange) and post (green) conditions. CR: completion rate, TP: throughput, TR: time to reach, PE: path efficiency, AS: average speed, OS: overshoot.

In summary, fatigue results in an increase in EMG amplitude and correspondingly in the control signals. However, the users can cope with the changed condition modulating the muscle activation level.

4 EXPERIMENTAL STUDY ON THE EFFECT OF ELECTRODE REPOSITIONING

The same protocol described in the above section was used to investigate experimentally the influence of donning and doffing, which includes change in electrode-skin contact.

Ten able-bodied subjects (ages: 26.10±2.17, 3 females and 7 males, all right handed) participated in this protocol which included two sessions. The position of the electrodes was outlined with a surgical marker for consistency across sessions. The positioning of the electrodes in the same position in the two different sessions aimed to investigate how the performance of the myoelectric control system change with changes in electrode impedance.

The experiment was divided in two sessions separated by two days. In the first session, subjects calibrated and tested the system (Optimal Subject-Specific 1, OSS1). The testing order was randomized and balanced among subjects. The obtained NNMF coefficients were manually sorted to

guarantee consistency across subjects and sessions. The second session involved three tests carried out in a randomized and balanced order among subjects. Three mappings were used: subject's own one from the previous session (Suboptimal Subject-Specific, SSS), subjects' own mapping after calibrating in session two (Optimal Subject-Specific 2, OSS2), and the mean of the of the other participants' mappings from session one, without including the evaluated subject, (Non-Subject-Specific, NSS). The aim of the experiment was to compare the differences in performance when subjects used their optimal mappings after a calibration session, and the performance achieved using suboptimal and subject-independent mappings.

The Normalized Dot Product (NDP) (Cheung et al., 2005; Muceli et al., 2014) was used to compare the estimated synergy matrixes and regression weights. Higher values of NDP indicate more similarity between the compared weights. The NDP was computed between subjects' mappings within OSS1 and OSS2, and within subjects' mappings between OSS1-OSS2, OSS1-NSS and OSS2-NSS. The aim of this analysis was to assess the differences between subjects' optimal mappings and the within-subject variability between the sessions.

To determine the differences in performance between the mappings, repeated measures analysis of variance (ANOVA) was used with 'Mapping' (OSS1, OSS2, SSS and NSS) as fixed factor for all the six metrics (the same used in the fatigue protocol). If the sphericity assumption was violated, as assessed by the Mauchy test, the Greenhouse-Geisser estimated correction (ε) was applied to satisfy the condition. Results were considered significant if $p \leq 0.05$.

Results

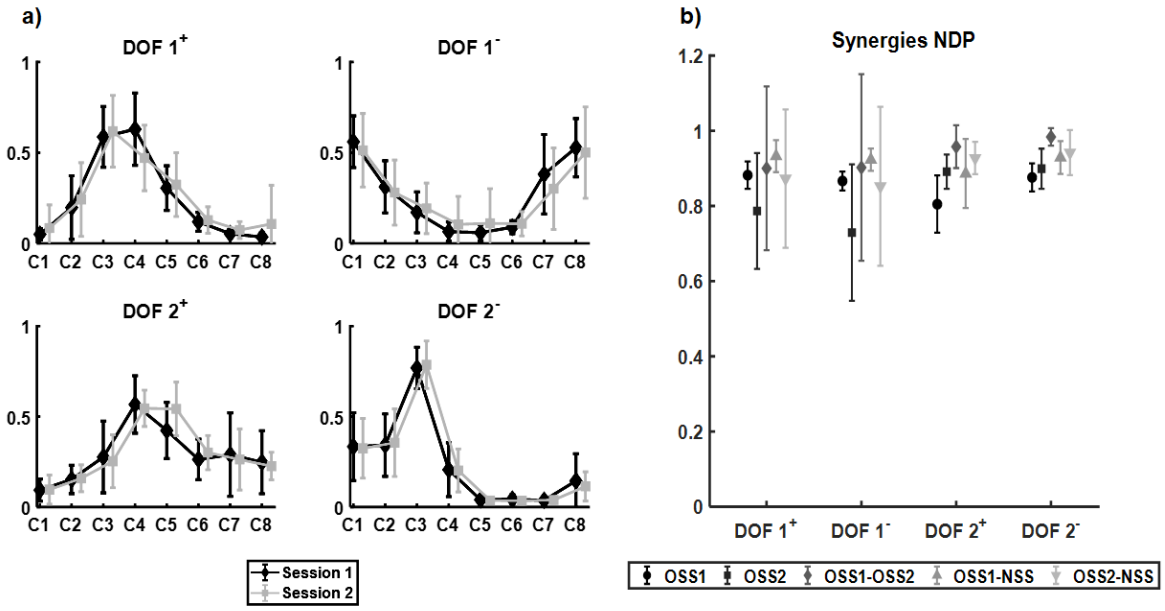

*Figure 9 a) Grand mean of the NNMF synergies for session 1 (black) and session 2 (*grey*) for both directions of each DOF. b) Normalized Dot Product (NDP) between the subjects optimal calibrations (OSS1 and OSS2), and within subjects between their optimal synergies (OSS1-OSS2) and the other subjects' mean (OSS1-NSS and OSS2-NSS). Both plots show the similarity between the obtained* synergies.

Figure 9 shows the grand mean of the obtained NNMF synergies per DOF. Similar profiles were obtained between the two session calibrations. On average, the analysis of the weights between subjects showed more similarity in session 1 than in session 2 (0.86 ± 0.04 and 0.83 ± 0.08,

respectively, for the mean across DOF). The within-subjects NDP between OSS had higher standard deviation for DOF 1 than DOF 2 (0.90 ± 0.22, 0.90 ± 0.25, 0.96 ± 0.06, 0.98 ± 0.02 for DOF 1+, DOF 1-, DOF 2+ and DOF 2-, respectively). The NDP obtained for the synergies (OSS1-NSS: 0.93 ± 0.04, 0.92 ± 0.03, 0.89 ± 0.09, 0.93 ± 0.04, and OSS2-NSS: 0.87 ± 0.18, 0.85 ± 0.21, 0.93 ± 0.04, 0.94 ± 0.06).

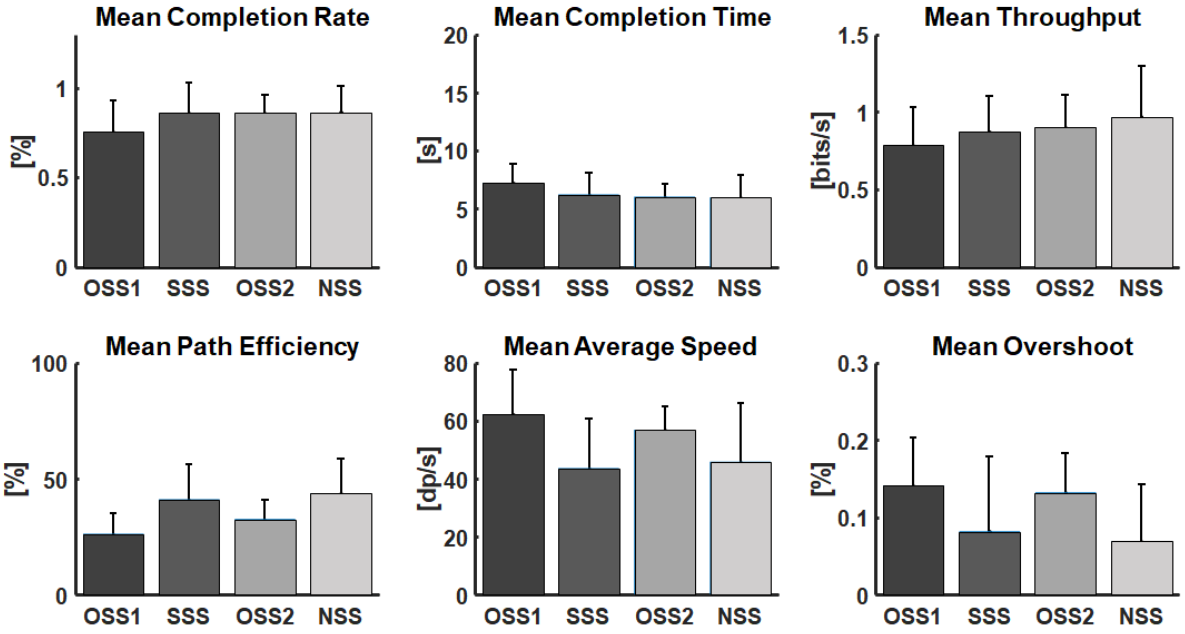

Figure 10 Overall mean performance across subjects for the Optimal Subject-Specific 1 (OSS1), Suboptimal Subject-Specific (SSS), Optimal Subject-Specific 2 (OSS2), and Non-Subject-Specific (NSS) test. Similar performance was obtained for all the mappings in all metrics, with no significant differences.

No significantly difference was observed for the following metrics (Figure 10): completion rate ($F(3,27) = 1.260$, $p = 0.308$), completion time ($F(3,27) = 0.971$, $p = 0.421$), throughput ($F(3,27) = 0.735$, $p = 0.540$), average speed ($F(1.816, 16.347) = 3.290$, $\varepsilon = 0.605$, $p = 0.067$) and overshoot ($F(3,27) = 2.383$, $p = 0.091$). Although, a significant difference was found in path efficiency ($F(3,27) = 4.063$, $p = 0.017$), the Bonferroni correction showed no significant difference among the pairs.

The similarity in performance in all considered cases suggestes that despite the within-subject differences in electrode-skin contact that may occurr with donning-doffing, the changes in EMG signal characteristics due to fatigue, and the differences in foream anatomy across subjects, user is able to adapt to changed conditions during real-time tasks.

REFERENCES

Bigland-Ritchie, B., Johansson, R., Lippold, O. C., Smith, S., and Woods, J. J. (1983). Changes in motoneurone firing rates during sustained maximal voluntary contractions. *J. Physiol.* 340, 335–346.

Cheung, V. C. K., D'Avella, A., Tresch, M. C., and Bizzi, E. (2005). Central and sensory contributions to the activation and organization of muscle synergies during natural motor

behaviors. *J. Neurosci.* 25, 6419–34. doi:10.1523/JNEUROSCI.4904-04.2005.

Enoka, R. M., Baudry, S., Rudroff, T., Farina, D., Klass, M., and Duchateau, J. (2011). Unraveling the neurophysiology of muscle fatigue. *J. Electromyogr. Kinesiol.* 21, 208–19. doi:10.1016/j.jelekin.2010.10.006.

Farrell, T. R., and Weir, R. F. (2007). The optimal controller delay for myoelectric prostheses. *IEEE Trans. Neural Syst. Rehabil. Eng.* 15, 111–8. doi:10.1109/TNSRE.2007.891391.

Fuglevand, A. J., Winter, D. A., and Patla, A. E. (1993). Models of recruitment and rate coding organization in motor-unit pools. *J. Neurophysiol.* 70, 2470–88. Available at: http://www.ncbi.nlm.nih.gov/pubmed/8120594.

Gazzoni, M., Camelia, F., and Farina, D. (2005). Conduction velocity of quiescent muscle fibers decreases during sustained contraction. *J. Neurophysiol.* 94, 387–94. doi:10.1152/jn.01182.2004.

Hahne, J. M., Biessmann, F., Jiang, N., Rehbaum, H., Farina, D., Meinecke, F. C., et al. (2014). Linear and Nonlinear Regression Techniques for Simultaneous and Proportional Myoelectric Control. *IEEE Trans. Neural Syst. Rehabil. Eng.* 22, 269–279. doi:10.1109/TNSRE.2014.2305520.

Hahne, J. M., Dähne, S., Hwang, H.-J. J., Müller, K. R., Parra, L. C., Dahne, S., et al. (2015). Concurrent Adaptation of Human and Machine Improves Simultaneous and Proportional Myoelectric Control. *IEEE Trans. Neural Syst. Rehabil. Eng.* 23, 618–627. doi:10.1109/TNSRE.2015.2401134.

Hahne, J. M., Markovic, M., and Farina, D. (2017). User adaptation in Myoelectric Man-Machine Interfaces. *Sci. Rep.* 7, 4437. doi:10.1038/s41598-017-04255-x.

Jiang, N., Englehart, K. B., and Parker, P. A. (2009). Extracting simultaneous and proportional neural control information for multiple-DOF prostheses from the surface electromyographic signal. *IEEE Trans. Biomed. Eng.* 56, 1070–80. doi:10.1109/TBME.2008.2007967.

Kamavuako, E. N., Scheme, E. J., and Englehart, K. B. (2014). Combined surface and intramuscular EMG for improved real-time myoelectric control performance. *Biomed. Signal Process. Control* 10, 102–107. doi:10.1016/j.bspc.2014.01.007.

Keenan, K. G., Farina, D., Maluf, K. S., Merletti, R., and Enoka, R. M. (2005). Influence of amplitude cancellation on the simulated surface electromyogram. *J. Appl. Physiol.* 98, 120–31. doi:10.1152/japplphysiol.00894.2004.

Keenan, K. G., Farina, D., Merletti, R., and Enoka, R. M. (2006). Influence of motor unit properties on the size of the simulated evoked surface EMG potential. *Exp. Brain Res.* 169, 37–49. doi:10.1007/s00221-005-0126-7.

Lee, D. D., and Seung, H. S. (2006). Algorithms for Non-negative Matrix Factorization. *Lect. Notes Comput. Sci.* 4029, 548–562. doi:10.1007/11785231_58.

Muceli, S., Jiang, N., and Farina, D. (2014). Extracting signals robust to electrode number and shift for online simultaneous and proportional myoelectric control by factorization algorithms. *IEEE Trans. Neural Syst. Rehabil. Eng.* 22, 623–33. doi:10.1109/TNSRE.2013.2282898.

Negro, F., and Farina, D. (2011). Decorrelation of cortical inputs and motoneuron output. *J. Neurophysiol.* 106, 2688–97. doi:10.1152/jn.00336.2011.

Vujaklija, I., Roche, A. D., Hasenoehrl, T., Sturma, A., Amsuess, S., Farina, D., et al. (2017). Translating research on myoelectric control into clinics – are the performance assessment methods adequate?